JACS
JOURNAL OF THE AMERICAN CHEMICAL SOCIETY

Article

Turning Au Nanoclusters Catalytically Active for Visible-Light-Driven CO2 Reduction through Bridging Ligands

Xiaofeng Cui, Jin Wang, Bing Liu, Shan Ling, Ran Long, and Yujie Xiong

J. Am. Chem. Soc., **Just Accepted Manuscript** • DOI: 10.1021/jacs.8b06723 • Publication Date (Web): 08 Nov 2018

ACS Publications

is published by the American Chemical Society. 1155 Sixteenth Street N.W., Washington, DC 20036

Turning Au Nanoclusters Catalytically Active for Visible-Light-Driven CO_2 Reduction through Bridging Ligands

Xiaofeng Cui,[†, ‡, ¶] Jin Wang,[†, ‡] Bing Liu,[†, ⊥] Shan Ling,[¶] Ran Long,[‡] and Yujie Xiong*[, ‡]

[‡]Hefei National Laboratory for Physical Sciences at the Microscale, iChEM (Collaborative Innovation Center of Chemistry for Energy Materials), School of Chemistry and Materials Science, and National Synchrotron Radiation Laboratory, University of Science and Technology of China, Hefei, Anhui 230026, P. R. China.

[¶]Anhui Key Laboratory of Photoelectric-Magnetic Functional Materials, School of Chemistry and Chemical Engineering, Anqing Normal University, Anqing, Anhui 246011, P. R. China.

[⊥]School of Chemical and Material Engineering, Jiangnan University, Wuxi, Jiangsu 214122, R. P. China.

KEYWORDS. Photocatalysis; gold cluster; catalytic sites; ligand; CO_2 reduction.

Supporting Information Placeholder

ABSTRACT: Developing visible-light photocatalytic materials is an ultimate goal for solar-driven CO_2 conversion. Au nanoclusters may potentially serve as the components for harvesting visible light, but can hardly perform the solar-driven CO_2 reduction due to the lack of catalytic sites. Herein, we report an effective strategy for turning Au nanoclusters catalytically active for visible-light CO_2 reduction, in which metal cations (Fe^{2+}, Co^{2+}, Ni^{2+} and Cu^{2+}) are grafted to the Au NCs using L-cysteine as a bridging ligand. The metal-S bonding bridge facilitates the electron transfer from Au NCs to metal cations so that the grafted metal cations can receive photo-induced electrons and work as catalytic sites for CO_2 reduction. The varied *d*-band centers and binding energies with CO_2 for different metal cations allow tuning electron transfer efficiency and CO_2 activation energy. Furthermore, the photostability of Au NCs-based catalyst can be significantly enhanced through the encapsulation with metal-organic frameworks. This work opens a new door for the photocatalyst design based on metal clusters, and sheds light on the surface engineering of metal clusters toward specific applications.

INTRODUCTION

Solar-driven conversion of CO_2 and H_2O into chemical fuels such as CH_4, CO/H_2 and methanol has been developed as a very promising approach to address current energy and environmental challenges.[1-6] To improve solar utilization, the visible light, which accounts for about 43% photons in the solar spectrum, should be harnessed for CO_2 photoreduction. Bandgap engineering and doping are the major approaches to tuning the spectral range of light harvesting by semiconductor – the key material to photocatalysis. Tailoring the parameters of semiconductor often causes the changes in electronic structures, charge separation and transfer, which in turn results in the variation of catalytic activity and selectivity.[7, 8] This complexity calls for the efforts to develop alternative materials which can harvest visible light through a different mechanism. Such a material platform would help reveal the fundamental mechanisms in photocatalytic CO_2 reduction.

Metal nanoclusters (NCs) are a class of ultrasmall nanoparticles as alternative materials to harvest solar light. In particular, thiolate-protected Au NCs can be obtained in solution phase through atomically precise synthesis, and possess high conductivity, strong visible-light response and abundant surface binding sites for cocatalysts and/or reaction species.[9, 10] As their particle sizes (~1 nm) approach to de Broglie wavelength, the continuous electronic bands in metallic nanoparticles would evolve to discrete energy levels.[11-13] For this reason, metal NCs exhibit analogous properties to molecular complexes whose light absorption can be readily tuned, and have emerged as visible-light harvesters in photocatalytic and photovoltaic systems.[14-17] Thus Au NCs are ideal candidates for absorbing visible light alternatively to semiconductor. Although some metal NCs have demonstrated their catalytic activity in reactions such as oxidation, hydrogenation and C-C coupling,[9, 10, 18-21] pristine Au NCs are almost inactive in photocatalytic reactions. The tight ligand capping on metal surface results in the lack of active sites for catalyzing reactions, and as such, the photogenerated electrons can hardly participate in reactions. To overcome this limitation, surface engineering should be performed on Au NCs to create active sites for CO_2 reduction.

In this article, we report a facile approach to the surface modification of glutathione-protected Au NCs (namely, Au-GSH NCs) through ligand grafting with L-cysteine (L-cys), which enables the effective immobilization of various transition metal cations as catalytic sites on surface. As such, the catalytic activity and selectivity in CO_2 photoreduction can be modulated by simply altering the grafted metal cations (Fe^{2+}, Co^{2+}, $Ni^{2+}$and Cu^{2+}). Density functional theory (DFT) calculations indicate that different active metals possess diverse *d*-band centers and adsorption energy with CO_2, altering the activity and selectivity of CO_2 reduction. As a proof of concept, the Au NCs grafted with Co^{2+} cations

achieve a rate of 3.54 μmol·g_{cat}^{-1}·h^{-1} and a selectivity up to 65.2% for CO production.

EXPERIMENTAL SECTION

Functionalization of Au-GSH NCs with L-cysteine (Au_c-C). The synthetic procedures for Au-GSH NCs are included in the Supporting Information. 10 mL of Au-GSH NCs dispersion (1 g·L^{-1}) was added into 10 mL of 2-(N-morpholino) ethane sulfonic acid (MES) buffer (3.9 mg·mL^{-1}) in a 50-mL round-bottom flask, which was then heated to 65 °C. Subsequently, 6 mg of 1-(3-dimethylaminopropyl)-3-ethylcarbodiimide hydrochloride (EDC) and 1.6 mg of N-hydroxysuccinimide (NHS) were added as catalysts to form amide bond between the carboxylic groups of the Au-GSH NCs and the amino groups of L-cys. After stirring for 15 min, 40 mg of L-cys was added in. The final mixture was stirred at 65 °C for 6 h. The resulting L-cys-modified Au-GSH NCs (Au_c-C) were collected by centrifugation at 8,000 rpm for 5 min and washed with deionized water three times. Finally, 5 mL of deionized water was added into the purified Au_c-C, and 30 μL of NaOH (30% wt) was added timely for better dispersing Au_c-C in aqueous solution.

Grafting with metal cations (Au_c-C-M). The grafting of metal cations was carried out right before photocatalytic reactions. A certain amount of metal cations (Fe^{2+}, Co^{2+}, Ni^{2+}or Cu^{2+}) were added into 10 mL of Au_c-C dispersion (1 g·L^{-1}) under vigorous stirring. Metal cations were immediately coordinated with the thiol of L-cys to serve as catalytic sites in photocatalytic reactions. The Au NCs grafted with metal cations were denoted as Au_c-C-M.

Photocatalytic CO_2 conversion measurements. The photocatalytic CO_2conversion measurement was performed in a home-made quartz reactor with a total volume of 50 mL. 1 mL of triethanolamine (TEOA) was added into 10 mL of pristine Au_c-C-Co solution (1 g·mL^{-1}) to sacrifice photogenerated holes. The mixture was bubbled with CO_2 about 30 min to eliminate air and form saturated CO_2 atmosphere. A 300-W Xe lamp (Solar edge 700, China) with a 420-nm long-wave-pass cut-off filter (λ≥420 nm) was used as a visible-light source. The power density was measured to be 100 mW cm^{-2}. The photocatalytic reaction was typically performed for 3h at room temperature and under ambient pressure. The amounts of CH_4, CO and H_2 evolved were determined using gas chromatograph (GC, 7890A, Ar carrier, Agilent). H_2 was detected using a thermal conductivity detector (TCD). CH_4 was measured by a flame ionization detector (FID). CO was converted to CH_4 by a methanation reactor and then analyzed by the FID. The isotope-labeled experiments were performed using $^{13}CO_2$ instead of $^{12}CO_2$, and the products were analyzed using gas chromatography-mass spectrometry (GC-MS, 7890A and 5975C, Agilent).

RESULTS AND DISCUSSION

The central concept of this work is to bridge light-harvesting Au NCs and catalytic metal sites with ligands. As a matter of fact, we can receive some inspirations from the applications of Au NCs as fluorescent probes in the detection of metal cations, in which the fluorescence of Au NCs is quenched by the efficient electron transfer from Au NCs to metal cations.[22-25] If the metal cations that receive the photogenerated electrons can catalyze CO_2 reduction, they would be able to serve as additional catalytic sites to Au NCs. In this work, we select water-soluble Au-GSH NCs as a model system owing to its intrinsic unique photochemical property and synthetic feasibility. The abundant surface ligands on Au-GSH NCs provide the opportunity for constructing catalytic sites through ligands modification.

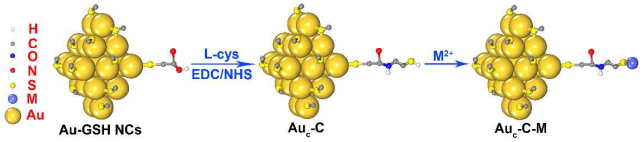

Figure 1. Schematic illustration for the process of modifying Au clusters with L-cys ligands (Au_c-C) and further grafting them with metal cations (Au_c-C-M).

The concept and preparation procedures are illustrated in Figure 1. Au-GSH NCs are facilely prepared through a simple one-pot method by slightly modifying the reported protocol, in which aqueous solutions of $HAuCl_4$ and GSH are mixed and allowed to react under gentle stirring at a temperature of 70 °C (see details in Supporting Information).[26] The lowest unoccupied molecular orbital (LUMO) and highest occupied molecular orbital (HOMO) energy levels of Au-GSH NCs are located at -0.63 V and 1.51 V (*vs.* RHE), which are thermodynamically favorable for CO_2 reduction and H_2O oxidation, respectively.[17] As indicated by matrix-assisted laser desorption/ionization time-of-flight (MALDI-TOF) mass spectrometry (Figure S1), this simple one-pot method can yield Au-GSH NCs with a size distribution ranging from Au_{24} to Au_{39}. The Au-GSH NCs are excellent absorbers to harvest visible light up to 500 nm as well as offer relatively high stability as compared with monodispersed Au NCs, which can improve photocatalytic activity and durability. The quantum yield of Au-GSH NCs may reach 15%, orders of magnitude higher than that of the reported Au-thiolate NCs (typically 0.001–0.1%).[26] The Au-GSH NCs display excellent stability, including storage in water at room temperature and elevated temperature (80 °C), in solutions of high salt concentration, and in common buffer solutions.[26] The capping ligands on Au-GSH NCs only provide -NH_2 and -COOH groups for anchoring transition metal cations, which have lower affinity as compared with -SH group. To bind catalytic sites more firmly on the surface of Au NCs, Au-GSH NCs are further functionalized with L-cys (namely, Au_c-C). This step is achieved through the formation of amide bond between the carboxylic groups of GSH and the amino groups of L-cys, catalyzed by 1-(3-dimethylaminopropyl)-3-ethylcarbodiimide hydrochloride (EDC) and N-hydroxysuccinimide (NHS).[27] The structure of Au NCs is well retained after the functionalization (see Figure S2), and the uncoordinated thiols introduced by L-cys provide a platform for anchoring metal cations onto the nanoclusters (namely, Au_c-C-M; M = Fe, Co, Ni and Cu).

To investigate whether the amide bond has been formed between Au-GSH NCs and L-cys, synchrotron radiation-based Fourier-transform infrared spectroscopy (FTIR) spectroscopy is employed to examine the samples. As shown in Figure 2a, pure GSH display three peaks of amide bond at 1655 cm^{-1} (C=O stretching), 1545 cm^{-1} (N–H bending) and 1397 cm^{-1} (C–N stretching). However, these characteristic peaks disappear after binding GSH to Au NCs (i.e., Au-GSH NCs),

most likely as the amide bonds on Au-GSH NCs are not infrared active. This feature has been reported for the amide bonds in GSH-protected nanoclusters.[28, 29] After grafting L-cys onto the Au-GSH NCs (i.e., Au_c-C), the peaks at 1660 cm^{-1} (C=O stretching), 1530 cm^{-1} (N–H bending) and 1390 cm^{-1} (C–N stretching) appear again, which can be ascribed to the characteristics for bending modes of newly formed amide bond between GSH and L-cys.[30] Moreover, the stretching vibration peak of N−H bond at 3000−3200 cm^{-1} is shifted toward higher frequency in Au_c-C with respect to bare L-cys, which is attributed to the inductive effect of electron-withdrawing group – carbonyl in amide. This verifies the formation of amide bond during the functionalization on Au-GSH NCs. This conclusion is further confirmed by X-ray photoelectron spectroscopy (XPS). As shown in Figure 2b, the Au4f XPS peaks for Au_c-C are shifted about 0.4 eV toward lower binding energy after grafting L-cys. This evidences the existence of L-cys ligands, as the electron donation by -NH_2 in the L-cys can increase the electron density of Au atoms.

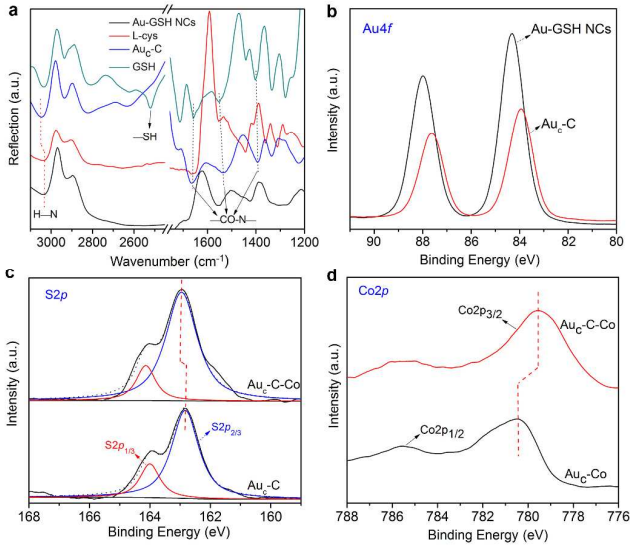

Figure 2. (a) FTIR spectra of Au-GSH NCs and Au_c-C in reference to L-cys and GSH. High-resolution XPS spectra of (b) Au4f in Au-GSH NCs and Au_c-C, (c) S2p in Au_c-C and Au_c-C-Co, and (d) Co2p in Au_c-Co and Au_c-C-Co.

To further examine whether this functionalization process results in ligand exchange, we employ ^{1}H nuclear magnetic resonance (NMR) spectroscopy to characterize the solution after the reaction of modifying Au-GSH NCs with L-cys for 6 h. As shown in Figure S3, no free GSH can be detected in the solution, which indicates that the ligand exchange between the L-cys and Au-GSH NCs should be negligible in this system. The Au_c-C is fully purified prior to the further coordination with metal cations so that no free L-cys or GSH is involved in the system (Figure S4). As determined by high-performance liquid chromatography (HPLC, Figure S5), the molar ratio of GSH to grafted L-cys is about 1:0.81 after the functionalization. It is also worth pointing out that Au-GSH NCs have not aggregated through cross coupling after the ligand modification as indicated by their light absorption (Figure S6). The undesired crosslinking is effectively suppressed by adding excess L-cys into Au-GSH NCs solution so that more L-cys molecules can be adsorbed onto the surface of Au-GSH NCs, which favors the reaction of GSH with the amine group of adsorbed L-cys.

The next question would be whether metal cations have been bound to the thiols of modified Au NCs. High-resolution XPS has been employed to provide the evidence. Here we take the earth abundant Co^{2+} as an example to demonstrate this approach, which can be coordinated with the thiols of Au_c-C to form Au_c-C-Co. As charge transfer should take place upon the coordination of thiols and Co^{2+} cations, we pay more attention to the XPS peak shift of S and grafted Co. The S2p XPS spectrum (Figure 2c) shows the S2$p_{1/3}$ and S2$p_{2/3}$ peaks with binding energies at 162.8 eV and 163.9 eV, respectively, which can be assigned to the thiols of GSH and/or L-cys.[31] After grafting Co^{2+}, the S2$p_{1/3}$ and S2$p_{2/3}$ peaks are shifted about 0.2 eV toward higher binding energy, which indicates the reduction in electron density of the S in Au_c-C-Co. Meanwhile, the peak of grafted Co2p (779.6 eV) is shifted toward opposite direction with respect to the Co^{2+} cations mixed with unmodified Au-GSH NCs (Au_c-Co, 780.4 eV) as shown in Figure 2d, revealing that the electron density of the Co atoms increases after grafting. These XPS peak shifts can be attributed to the coordination of Co^{2+} with thiol which causes the migration of electrons from S atoms to Co atoms.[31] The XPS characterization thus confirms the effective binding of Co cations to Au NCs though L-cys ligands.

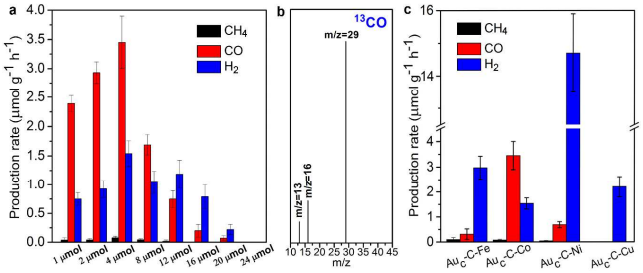

Figure 3. (a) Average production rates of CH_4, CO and H_2 in light-driven CO_2 reduction with H_2O in the presence of TEOA, catalyzed by 10-mg Au_c-C grafted with different amounts of Co^{2+}. (b) Mass spectra of ^{13}CO (m/z = 29) produced over Au_c-C-Co in light-driven reduction of $^{13}CO_2$. (c) Average production rates of CH_4, CO and H_2 in light-driven CO_2 reduction with H_2O in the presence of TEOA, catalyzed by 10-mg Au_c-C grafted with 4-μmol Fe^{2+}, Co^{2+}, Ni^{2+} or Cu^{2+}. The irradiation is performed with visible light ($\lambda \geq 420$ nm) with a power density of 100 mW·cm^{-2} for 3 h.

We are now in a position to assess the performance of grafted metal cations as catalytic sites. The evaluation is performed for our catalysts with CO_2 and H_2O under visible-light irradiation, using triethanolamine (TEOA) to sacrifice photogenerated holes. As shown in Table S1, the Au-GSH NCs and Au_c-C without metal cations anchored do not exhibit catalytic activity for CO_2 reduction. As Au NCs are grafted with Co^{2+} through L-cys (Au_c-C-Co, Figure 3a), they can be turned catalytically active for CO_2 reduction. In contrast, simply mixing Au-GSH NCs with metal cations does not generate the catalytic activity, indicating that the L-cys bridging is the key to electron transfer from light-harvesting center to catalytic sites. To trace the carbon source of CO, isotopic $^{13}CO_2$ is used as the reactant to perform the photocatalytic reaction under identical conditions. As

indicated by mass spectrometry (Figure 3b), the peak at m/z= 29 can be ascribed to ^{13}CO. It confirms that the CO indeed originates from photocatalytic CO_2 reduction.

Furthermore, a volcano tendency (Figure 3a) has been observed for the photocatalytic activity by continuously increasing the amount of Co^{2+} cations from 1 to 16 μmol. At the volcano maximum (4-μmol Co^{2+}), the reduction of CO_2 to CO can be achieved with an evolution rate of 3.45 $\mu mol \cdot g_{cat}^{-1} \cdot h^{-1}$ and a selectivity of 65.2% (Table S1). In addition to a small amount of produced CH_4, the major side reaction is the reduction of protons in H_2O to H_2. The synthesis gas with a CO/H_2 ratio between 0.5 and 1 is the desired gas source for the thermochemical synthesis of methanol and Fischer-Tropsch reactions in the existing industrial processes. In general, more catalytic sites can offer higher activity; however, the photocatalytic activity is sharply declined together with the reduced CO selectivity as the amount of Co^{2+} is increased beyond 4 μmol. This deteriorative performance may result from the redundantly free Co^{2+} cations in solution (Figure S7), as we have not purified the Au_c-C-Co NCs after the coordination with metal cations. The free Co^{2+} cations may act as a shuttle redox mediator for the recombination of photogenerated electrons and holes to reduce photocatalytic activity.[16] The activity for CO_2 reduction is more affected by free Co^{2+} than H_2 generation as proton reduction can more easily take place than CO_2 reduction (the rate-limiting step for CO_2 reduction $CO_2 + e^- \rightarrow CO^{2\bullet-}$, −1.85V *versus* SHE; water reduction $2H_2O(l) + 2e^- \rightarrow H_2(g) + 2OH^-(aq)$, −0.414 V *versus* SHE). As the Co^{2+} loading reaches 24 μmol, both H_2 production and CO_2 reduction are totally shut off. After removing the free Co^{2+}, the photocatalytic activity can be improved as shown in Figure S8.

Another merit of our synthetic scheme is the variety of metal cations that can be readily grafted to Au NCs, which allows correlating catalytic performance with metal sites. Figure 3c shows the average production rates of CH_4, CO and H_2 by Au_c-C grafted with different metal cations (see the actual loading amounts in Table S2). Apparently, the other three catalytic centers (Fe^{2+}, Ni^{2+} and Cu^{2+}) are more favorable to produce H_2, whose H_2 selectivity even reach 81.11%, 94.51% and 100%, respectively. Notably, Au_c-C-Ni exhibits the highest activity with the average rate of electron consumption ($R_{electron}$) reaching 31.1 $\mu mol \cdot g_{cat}^{-1} \cdot h^{-1}$. Table S3 summarizes the performance comparison of our samples with the reported cases.

To appreciate the roles of surface modification and metal cation grafting, we collect spectroscopic information for light absorption and charge behavior. The absorption spectrum in Figure S6 indicates that Au_c-C is an excellent absorber to harvest visible light up to 500 nm, whose absorption profile has not been altered by grafting various metal cations. Given the well maintained light absorption, we further look into the transfer of photogenerated electrons from Au-GSH NCs to the grafted metal sites, whose efficiency should be a crucial factor for photocatalytic reactions according to the Marcus theory. To correlate the electron-transfer process with metal sites, we employ steady and transient photoluminescence (PL) spectroscopy to examine the samples. The steady-state PL of Au NCs is gradually quenched by increasing the loading amounts of Co^{2+} cations (Figure S9). Furthermore, various metal cations display different quenching effects on the PL of Au NCs (Figure S10). Cu^{2+} exhibits an exceptionally strong quenching effect, and nearly fully quenches the PL at the amount of 4 μmol. Co^{2+} and Ni^{2+} quench the PL 52.1% and 49.7% at the same amount of metal cations, respectively, while no apparent quenching can be observed for the addition of Fe^{2+}. The electron transfer between clusters and metal cations can induce such a quenching effect on the PL of metal NCs. This argument is supported by the PL measurements for the samples in the absence of bridging ligands. The PL of the unmodified Au-GSH NCs (Au_c) whose strong photoemission exhibits a maxima around 630 nm can hardly be quenched by the addition of Fe^{2+}, Co^{2+} and Ni^{2+} cations (Figure S11). The only exception is the distinct quenching observed for the addition of Cu^{2+} cations. A previous report indicates a similar case caused by aggregation-induced fluorescence quenching through the complexation of Cu^{2+} with GSH rather than electron transfer.[32]

To look into the origin of PL quenching, normalized time-resolved PL decay is conducted with a pulsed laser excitation at λ = 365 nm (Figure 4a). The decay traces can be fitted using triexponential decay kinetics with the parameters listed in Table S4. Similarly to the decay tendency in steady-state PL spectra, Au_c-C-Cu, Au_c-C-Co and Au_c-C-Ni show fast decay with average PL decay time ($T_{average}$) of 0.08 ns, 0.51 ns and 0.89 ns, respectively, while Au_c-C-Fe exhibits comparable $T_{average}$ to Au_c-C. Nevertheless, electron transfer is not the only factor responsible for PL decay. It is known that the contributions of τ_1 and τ_2 are more related to charge transfer.[33, 34] Although the τ_1 and τ_2 for Au_c-C-Cu are smaller than those for Au_c-C-Co, its PL decay is more governed by τ_3.

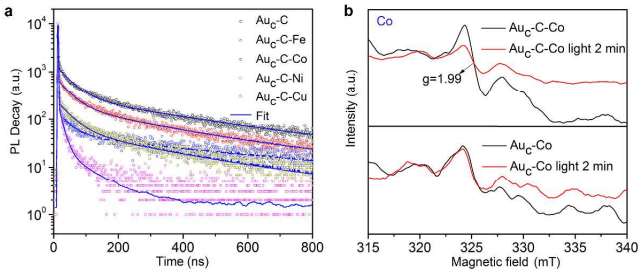

Figure 4. (a) Time-resolved transient fluorescence spectra of Au-GSH NCs modified with L-cys (Au_c-C) and Au_c-C grafted with different metal cations (Fe^{2+}, Co^{2+}, Ni^{2+} and Cu^{2+}, 4 μmol) in aqueous solution, excited at 455 nm. (b) ESR spectra of Au_c-Co (lower) and Au_c-C-Co (upper) in dark or under light irradiation for 2 min.

We also employ electron spin resonance (ESR) spectroscopy to probe the information for trapped electrons at metal sites. As shown in Figure 4b, strong signals are observed at g=1.99, which can be ascribed to high-spin state of Co^{2+}.[35] The peak shift for Au_c-C-Co is caused by the interaction between Au_c-C and Co, which further confirms the strong coordination ability of functionalized Au_c-C. Furthermore, the ESR signal intensity for Au_c-C-Co is significantly weakened after light irradiation, while no distinct change is observed for Au_c-Co in the absence of L-cys bridge. This Co ESR signal decay can be assigned to the lowered spin state during the reduction of Co^{2+} by photoexcited electrons.[36] Given the role of Co^{2+} as an electron acceptor, we propose that the grafted Co^{2+} should be the active site for CO_2 reduction. A similar ESR signal change with light irradiation is also observed for the Fe^{2+}, Ni^{2+} and Cu^{2+} cations that are grafted to

Au NCs through the L-cys bridging ligand (Figure S12). This characterization also indicates that the L-cys bridging ligand is the key to electron transfer.

Upon acquiring the information of electron transfer, we further examine the electronic structures of metal sites through DFT calculations as the electron transfer is not the only factor determining photocatalytic activity and selectivity. Based on the optimized structural models in Figure S13, we obtain the *d*-band centers (ε_d) of 4 different metal sites. The *d*-band center is defined as the average energy of *d*-band, which characterizes the ability to inject electrons into the adsorbate from the *d*-band of metal.[37] In general, electrons can be more easily injected into the antibonding orbitals when the *d*-band center is closer to the Fermi level, making catalyst surface more reactive.[37-39] Figure 5a shows that the calculated *d*-band centers (ε_d) for the Au_c-C grafted with Fe^{2+}, Co^{2+}, Ni^{2+}, and Cu^{2+}, whose distance to the Fermi level (E_f) follows the order: Au_c-C-Ni (-1.61) < Au_c-C-Co (-2.13) < Au_c-C-Fe (-2.63) < Au_c-C-Cu (-3.18). From the viewpoint of active sites, Ni^{2+} and Co^{2+} should offer higher catalytic activity in reactions. Taken together, the PL characterization and DFT calculation show that the photocatalytic performance of Au_c-C-Fe and Au_c-C-Cu is largely limited by their low efficiency of electron transfer and/or low catalytic activity of active sites, respectively.

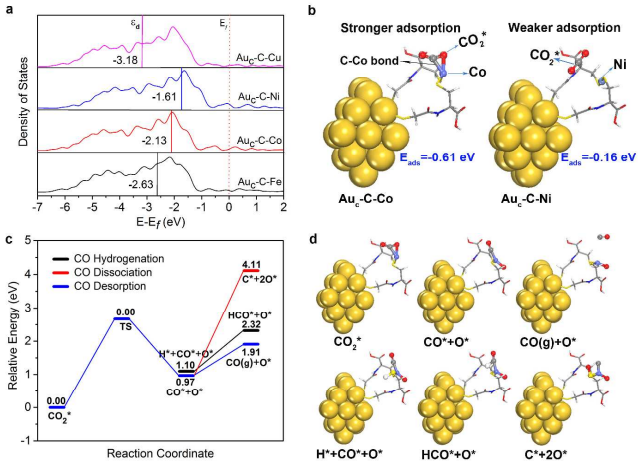

Figure 5. (a) Projected density of states (PDOS) of the *d*-orbitals of surface atoms for Au_c-C-Fe, Au_c-C-Co, Au_c-C-Ni and Au_c-C-Cu. The red dashed lines represent the Fermi level, and the solid lines indicate the *d*-band centers (ε_d). (b) Models for CO_2 adsorption on Au_c-C-Co surface (left) and Au_c-C-Ni surface (right). (c) Energy profiles for CO formation and desorption, CO dissociation, and CO hydrogenation on Au_c-C-Co surface. (d) Calculated structures of CO formation and desorption, CO dissociation, and CO hydrogenation on Au_c-C-Co surface.

In addition to photocatalytic activity, product selectivity is a key parameter to CO_2 reduction. Au_c-C-Co and Au_c-C-Ni show very different selectivity in CO_2 reduction, which can be attributed to the varied adsorption strength of CO_2 to metal sites. As shown in Figure 5b, the CO_2 adsorption energy on Au_c-C-Co is calculated to be -0.61 eV with the formation of C-Co bond. In contrast, the adsorption of CO_2 on Au_c-C-Ni is relatively weak with an adsorption energy of -0.16 eV. In particular, the absence of C-Ni bonding indicates a weak physisorption. The chemisorption of CO_2 on Au_c-C-Co favors the reduction of CO_2 and improves the selectivity of CO_2 reduction over proton reduction.

To depict the reaction pathway on Au_c-C-Co, we calculate the energies for CO formation, desorption, dissociation and hydrogenation on Au_c-C-Co surface. As displayed in Figure 5c and 5d, the desorption of CO from surface requires a lower energy (0.94 eV) than the dissociation (3.14 eV) or hydrogenation (1.22 eV) of CO molecule. For this reason, the CO formed on Au_c-C-Co would preferentially be desorbed from surface and produce CO gas rather than undergo further reactions. This improves the selectivity of CO production by Au_c-C-Co catalysts as observed in our experiments. In particular, the formation of CH_4, which requires the cleavage of C-O bond and the formation of C-H bond, is limited by the high energy barriers for CO dissociation and hydrogenation.

To examine the durability of our catalysts, we have performed a test in 3 successive cycles each of which takes 3 hours. Unfortunately, the NC-based catalysts exhibit frustrating photostability in the cycling test, and become nearly inactive after the 3 cycles (Figure S14). Transmission electron microscopy (TEM) characterization (Figure S15) reveals that Au NCs have been aggregated and grown from 1.53 nm up to Au nanoparticles with an average diameter of 3.34 nm after the 3 cycles, together with emerging surface plasmon resonance (SPR) peaks for Au nanoparticles (Figure S16). Similar situation has been found for the Au NCs used as a photosensitizer.[17, 40]

To prevent NC agglomeration and enhance photostability, we employ Zn(2-methylimidazole)$_2$ (ZIF-8) framework as an encapsulation shell to protect Au_c-C-Co (Figure S17 and S18). Cycling test indicates that the photostability is remarkably improved by the ZIF-8 encapsulation. No obvious activity decay is observed during four 3-hour reaction cycles (Figure S19), as both ZIF-8 coating and Au_c-C-Co can be well maintained (Figure S20 and S21). Thus the encapsulation of Au NCs with metal-organic frameworks (MOFs) is an effective strategy for enhancing their photostability. However, in the case of ZIF-8, the activity and CO selectivity are lowered after the encapsulation. The cladding shell of ZIF-8 hinders the mass transfer of CO_2 and TEOA to lower the catalytic activity. Meanwhile, the CO selectivity is most likely reduced by the presence of Zn in ZIF-8, which demonstrates its role as active sites to produce H_2 (Figure S19). It is anticipated that these deficiencies in our proof-of-concept experiments can be overcome by coating a porous shell with optimal channels and appropriate metal atoms.

To demonstrate the efficacy of our approach to Au NCs, we also employ a monodispersed $Au_{25}(SG)_{18}$ system to perform photocatalytic CO_2 reduction. After modified with L-cys and grafted with Co^{2+}, the Au_{25}-C-Co shows good photocatalytic activity (Figure S22), proving that our reported approach should be applicable to various NCs. This monodispersed system also provides a well-defined platform for examining the grafting of L-cys to Au NCs through MALDI-TOF mass spectrometry. As shown in Figure S23, this characterization suggests that $Au_{25}(SG)_{18}$ is modified with L-cys and well maintained during the functionalization.

Another key point to the universal feature of our method is the selection of bridging ligands. We modify Au-GSH NCs with another ligand – 3-mercaptopropionic acid (MPA) which has a similar molecular structure to L-cys except the absence

of amine in MPA, and then graft Co^{2+} onto the NCs through MPA. The obtained Au_c-MPA-Co shows good activity for light-driven CO_2 reduction (Figure 24), indicating that MPA also can work as an electron transporter. In our approach, the bridging ligand should be a bifunctional linker molecule that possesses one functional group (e.g., carboxylate and amine) for binding with Au NCs and one thiol as a terminal group for coordination with metal cations. We further compare the photocatalytic activity of Au_c-C-Co and Au_c-MPA-Co, and identify that the activity of Au_c-MPA-Co is slightly higher than that of Au_c-C-Co. The nitrogen atom possesses a stronger negative induction effect owing to its high electronegativity than sulfur, which makes the charge density of thiol in L-cys lower than that in MPA. DFT calculation reveals that the binding energy of S–Co in the coordination of L-cys with Co (-1.13 eV) is lower than that for MPA (-1.51 eV). We thus assume that the stronger S–metal cation interaction promotes the photocatalytic activity.

CONCLUSION

In conclusion, we have developed a facile surface modification method to construct catalytic sites on inert Au NCs for photocatalytic CO_2 reduction, in which various metal cations can be grafted to Au NCs through bridging ligands. As demonstrated by our characterizations, the metal cations can accept photogenerated electrons from Au NCs through the bridging ligands and serve as catalytic sites for CO_2 reduction. Given these functions, the selection of metal cations largely impacts on the efficiency of electron transfer from light-harvesting centers to catalytic sites, the ability of donating electrons to reaction species, and the adsorption of reaction species. The impact in turn alters the activity and selectivity of photocatalytic CO_2 reduction. This work demonstrates an effective surface engineering strategy for bridging catalytic sites with light-harvesting centers, and offers a model system for investigating the complex effects from catalytic sites toward photocatalyst design. From the viewpoint of practical applications, the agglomeration-induced instability of nanoclusters has to be overcome, to which the integration with MOFs may provide a solution.

ASSOCIATED CONTENT

Supporting Information. Detailed experimental section, characterization methods, and additional material characterizations. This material is available free of charge via the Internet at http://pubs.acs.org.

AUTHOR INFORMATION

Corresponding Author

*yjxiong@ustc.edu.cn

Author Contributions

‡These authors contributed equally.
The manuscript was written through contributions of all authors.

Notes

The authors declare no competing financial interest.

ACKNOWLEDGMENT

This work was financially supported in part by National Key R&D Program of China (2017YFA0207301), NSFC (21725102, 21603003, 21471141, U1532135), Anhui Provincial Natural Science Foundation (1708085QB43), Anhui Province Natural Science Key Foundation (KJ2016A861), CAS Key Research Program of Frontier Sciences (QYZDB-SSW-SLH018), CAS Interdisciplinary Innovation Team, and Innovative Program of Development Foundation of Hefei Center for Physical Science and Technology (2016FXCX003). FTIR characterization was performed at the Infrared Spectroscopy and Microspectroscopy Endstation (BL01B) in the National Synchrotron Radiation Laboratory (NSRL) in Hefei, China.

REFERENCES

1. Halmann, M. *Nature* **1978**, *275*, 115.
2. Inoue, T.; Fujishima, A.; Konishi, S.; Honda, K. *Nature* **1979**, *277*, 637.
3. Aresta, M.; Dibenedetto, A.; Angelini, A. *Chem. Rev.* **2014**, *114*, 1709.
4. White, J. L.; Baruch, M. F.; Pander, J. E.; Hu, Y.; Fortmeyer, I. C.; Park, J. E.; Zhang, T.; Liao, K.; Gu, J.; Yan, Y.; Shaw, T. W.; Abelev, E.; Bocarsly, A. B. *Chem. Rev.* **2015**, *115*, 12888.
5. Gao, C.; Wang, J.; Xu, H. X.; Xiong Y. J. *Chem. Soc. Rev.* **2017**, *46*, 2799.
6. Lingampalli, S. R.; Ayyub, M. M.; Rao, C. N. R. *ACS Omega* **2017**, *2*, 2740.
7. Bai, S.; Jiang, J.; Zhang Q.; Xiong, Y. J. *Chem. Soc. Rev.* **2015**, *44*, 2893.
8. Jiao, Y.; Zheng, Y.; Chen, P.; Jaroniec, M.; Qiao, S. Z. *J. Am. Chem. Soc.* **2017**, *139*, 18093.
9. Li, G.; Jin, R. C. *Acc. Chem. Res.* **2013**, *46*, 1749.
10. Jin, R. C.; Zeng, C. J.; Zhou, M.; Chen, Y. X. *Chem. Rev.* **2016**, *116*, 10346.
11. Philip, R.; Chantharasupawong, P.; Qian, H. F.; Jin, R. C.; Thomas, J. *Nano Lett.* **2012**, *12*, 4661.
12. Zhu, M. Z.; Aikens, C. M.; Hollander, F. J.; Schatz, G. C. Jin, R. C. *J. Am. Chem. Soc.* **2008**, *130*, 5883.
13. Kogo, A.; Sakai, N.; Tatsuma, T. *Nanoscale* **2012**, *4*, 4217.
14. Wang, H. K.; Chen, F.Y.; Li, W.Y.; Tian, T. *J. Power Sources* **2015**, *287*, 150.
15. Sakai, N.; Tatsuma, T. *Adv. Mater.* **2010**, *22*, 3185.
16. Chen, Y.S.; Choi, H. B.; Kamat, P.V. *J. Am. Chem. Soc.* **2013**, *135*, 8822.
17. Chen, Y. S.; Kamat, P. V. *J. Am. Chem. Soc.* **2014**, *136*, 6075.
18. Gaur, S.; Wu, H.; Stanley, G. G.; More, K.; Kumar, C. S.; Spivey, J. J. *Catal. Today* **2013**, *208*, 72.
19. Zhu, Y.; Qian, H.; Drake, B. A.; Jin, R. *Angew. Chem. Int. Ed.* **2010**, *49*, 1295.
20. Li, G.; Jiang, D. E.; Liu, C.; Yu, C.; Jin, R. *J. Catal.* **2013**, *306*, 177.
21. Chen, W.; Chen, S. *Angew. Chem. Int. Ed.* **2009**, *48*, 4386.
22. Shang , L.; Dong, S. J.; Nienhaus, G. U. *Nano Today* **2011**, *6*, 401.
23. Zhang, L. B.; Wang, E. K. *Nano Today* **2014**, *9*, 132.
24. Shang, L.; Dong, S. J. *J. Mater. Chem.* **2008**, *18*, 4636.
25. Durgadas, C. V.; Sharmaa C. P.; Sreenivasan, K. *Analyst* **2011**, *136*, 933.
26. Luo, Z. T.; Yuan, X.; Yu, Y.; Zhang, Q. B.; Leong, D. T.; Lee, J. Y.; Xie, J. P. *J. Am. Chem. Soc.* **2012**, *134*, 16662.
27. Zhang, K.; Zhou, H. B.; Mei, Q. S.; Wang, S. H.; Guan, G. J.; Liu, R. Y.; Zhang, J.; Zhang, Z. P. *J. Am. Chem. Soc.* **2011**, *133*, 8424.
28. Le Guével, X; Spies, C.; Daum, N.; Jung, G.; Schneider, M. *Nano Res.* **2012**, *5*, 379.
29. Li, H.; Cui, Z.; Han, C. *Sensor. Actuat. B* **2009**, *143*, 87.
30. Tamami, B.; Yeganeh, H. *Eur. Polym. J.* **2002**, *38*, 933.
31. Berner, S.; Lidbaum, H.; Ledung, G.; Åhlund, J.; Nilson, K.; Schiessling, J.; Gelius, U.; Bäckvall, J.E.; Puglia, C.; Oscarsson, S. *Appl. Surf. Sci.* **2007**, *253*, 7540.
32. Chen, W. B.; Tu, X. J.; Guo, X. Q. *Chem. Commun.* **2009**, *13*, 1736.
33. Xu Y. F.; Yang M. Z.; Chen B. X.; Wang X. D., Chen H. Y.; D. B.; Su C. Y. *J. Am. Chem. Soc.* **2017**, *139*, 5660.

34. Lightcap I. V.; Kamat P. V. *J. Am. Chem. Soc.* **2012**, *134*, 7109.
35. Ishihara, T.; Akbay, T.; Furutani, H.; Takita Y. *Solid State Ion.* **1998**, 113–115, 585.
36. Zhang, H. B.; Wei, J.; Dong, J. C.; Liu, G. G.; Shi, L.; An, P. F.; Zhao, G. X.; Kong, J. T.; Wang, X. J.; Meng, X. G.; Zhang, J.; Ye, J. H. *Angew. Chem. Int. Ed.* **2016**, *55*, 14310.
37. Miller, S. D.; Kitchin, J. R. *Surf. Sci.* **2009**, *603*, 794.
38. Li, J.; Croiset, E.; Ricardez-Sandoval, L. *J. Mol. Catal. A: Chem.* **2012**, *365*, 103.
39. Huo, C. F.; Li, Y. W.; Wang, J.; Jiao, H. *J. Am. Chem. Soc.* **2009**, *131*, 14721.
40. Xiao, F. X.; Zeng, Z.; Hsu, S. H.; Hung, S. F.; Chen, H. M.; Liu, B. *ACS Appl. Mater. Interf.* **2015**, *51*, 28105.

SYNOPSIS TOC

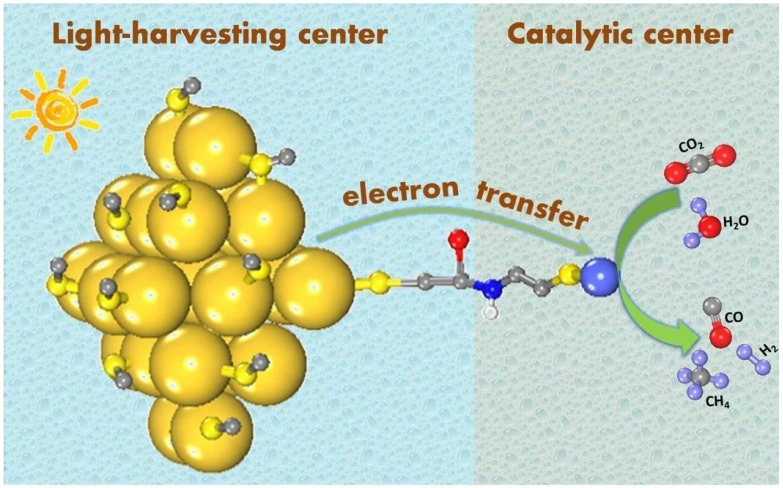

Gold nanocluster grafted with metal cations